

**Local atomic and electronic structure in LaMnO<sub>3</sub> across the orbital ordering transition**

Raquel A. Souza

*Laboratório Nacional de Luz Síncrotron (LNLS), P.O. Box 6192, 13084-971, Campinas, São Paulo, Brazil and Instituto de Física Gleb Wataghin, IFGW-UNICAMP, Campinas, SP, Brazil*

Narcizo M. Souza-Neto

*Laboratório Nacional de Luz Síncrotron (LNLS), P.O. Box 6192, 13084-971, Campinas, São Paulo, Brazil and Departamento de Física dos Materiais e Mecânica, DFMT-IF-USP, São Paulo, SP, Brazil*

Aline Y. Ramos\*

*Laboratório Nacional de Luz Síncrotron (LNLS), P.O. Box 6192, 13084-971, Campinas, São Paulo, Brazil and Laboratoire de Minéralogie-Cristallographie de Paris, LMCP-UMR 7590-CNRS, Paris, France*

Hélio C. N. Tolentino

*Laboratório Nacional de Luz Síncrotron (LNLS), P.O. Box 6192, 13084-971, Campinas, São Paulo, Brazil*

Eduardo Granado

*Laboratório Nacional de Luz Síncrotron (LNLS), P.O. Box 6192, 13084-971, Campinas, São Paulo, Brazil and Instituto de Física Gleb Wataghin, IFGW-UNICAMP, Campinas, SP, Brazil*

(Received 19 July 2004; revised manuscript received 30 September 2004; published 27 December 2004)

The local atomic disorder and electronic structure in the environment of manganese atoms in LaMnO<sub>3</sub> has been studied by x-ray absorption spectroscopy over a temperature range (300–870 K) covering the orbital ordering transition (~710 K). The Mn–O distance splitting into short and long bonds (1.95 and 2.15 Å) is kept across the transition temperature, so that the MnO<sub>6</sub> octahedra remain locally Jahn-Teller distorted. Discontinuities in the Mn local structure are identified in the extended x-ray fine structure spectra at this temperature, associated with a reduction of the disorder in the superexchange angle and to the removal of the anisotropy in the radial disorder within the coordination shell. Subtle changes in the electronic local structure also take place at the Mn site at the transition temperature. The near-edge spectra show a small drop of the Mn 4*p* hole count and a small enhancement in the pre-edge structures at the transition temperature. These features are associated with an increase of the covalence of the Mn–O bonds. Our results shed light on the local electronic and structural phenomena in a model of order-disorder transition, where the cooperative distortion is overcome by the thermal disorder.

DOI: 10.1103/PhysRevB.70.214426

PACS number(s): 75.47.Lx, 61.10.Ht, 71.90.+q, 64.70.Kb

**I. INTRODUCTION**

The lanthanum manganite and its doped perovskite alloys La<sub>1-x</sub>A<sub>x</sub>MnO<sub>3</sub> (with A=Ca,Sr,Ba) have attracted much attention in the last decade, in large part due to the potential applications of the so-called colossal magnetoresistance.<sup>1</sup> The unusual physical properties of these compounds arise from intricate interrelations between spin, charge, and local structure. In spite of the large experimental and theoretical efforts of the scientific community many of these interrelations remain not elucidated. In the LaMnO<sub>3</sub> compound itself many questions remain to be addressed. At room temperature LaMnO<sub>3</sub> is an antiferromagnetic semiconductor and crystallizes in an orthorhombic variant of the cubic perovskite structure space group *Pbnm*. The MnO<sub>6</sub> octahedra in LaMnO<sub>3</sub> are distorted due to the Jahn-Teller (JT) effects of the Mn<sup>3+</sup>(*t*<sub>2g</sub><sup>3</sup>*e*<sub>g</sub><sup>1</sup>) and the Mn–O distances are split into two groups. The manganese atoms are coupled ferromagnetically in the *ab* plane and antiferromagnetically along the *c* axis and an orbital ordering takes place. In the basal *ab* plane long and short Mn–O bonds alternate. The apical and basal short bonds have different length (≈1.91 Å and ≈1.97 Å,

respectively); however, this additional splitting is small for local probes such as real-space high-resolution diffraction<sup>2–4</sup> and extended x-ray absorption fine structure (EXAFS).<sup>5–7</sup> The local radial distribution is thus seen as made of a single distance at (Mn–O)<sub>s</sub> ≈ 1.94 Å, separated from the long distance long bond (Mn–O)<sub>l</sub> ≈ 2.15 Å. LaMnO<sub>3</sub> undergoes a transition at *T*\* ≈ 710–750 K from the JT-distorted orthorhombic phase to a high-temperature nearly cubic phase.<sup>8</sup> The space group *Pbnm* remains the same in both phases, but the cell distortion is nearly removed and the orbital ordering disappears in the high-temperature phase. The transition is accompanied by abrupt changes in the electrical resistivity, thermoelectric power, and Weiss constant.<sup>9</sup>

At the local scale two scenarios may be proposed: symmetrization of the distorted octahedra MnO<sub>6</sub> or an order-disorder transition, where the local distortion is maintained. From thermodynamic calculations it has been shown<sup>10</sup> that the thermal energy at *T*\* is small with respect to the gain associated to the lift of the *e*<sub>g</sub> levels degeneracy, so that this transition will hardly correspond to a removal of the octahedral distortion. The transition would happen as an order-disorder transition in the sequence of the distorted octahedra.

Experimentally, two early works from Raman spectroscopy<sup>11</sup> and from the analysis of the overall disorder in the EXAFS data across  $T^*$  (Ref. 12) supported the hypothesis of the upkeep of the local JT distortion. On the other hand, the hypothesis that the local JT distortion may vanish and the Mn–O distances collapse was sustained by the work in thin  $\text{LaMnO}_3$  films.<sup>13</sup> The two distances found by the fitting procedure<sup>13</sup> collapse into a single one above a given temperature in a similar way as the cell parameters. More recently, Sánchez *et al.*<sup>14</sup> have reached opposite conclusions from their x-ray absorption study in  $\text{LaMnO}_3$  polycrystals.

There have been various works using x-ray absorption spectroscopy (XAS), shedding light on the nature of the Jahn-Teller distortion, electronic states, thermal behavior, and disorder in manganites.<sup>5–7,12,14–21</sup> The thermal and structural disorder enters equivalently in the theory and in the data analysis where the overall disorder is usually expressed by a Debye Waller-like factor (DWF). The thermal disorder depends on the dynamical properties of the lattice. It presents a smooth continuous increase with the temperature that can be modeled using models of correlated vibrations.<sup>22</sup> The structural local disorder accounts for bond length dispersion and site distortions that, in the absence of structural transition, are temperature independent. At high temperatures, the EXAFS signal is strongly damped by the thermal disorder. The limited available analysis range reduces the  $R$  resolution and closely correlated fitting parameters cannot always be unambiguously resolved.<sup>5</sup> In addition, the structural disorder associated with the long and short Mn–O bonds are significantly different<sup>6,7</sup> and the thermal behavior of the DWF may not be correlated. To avoid misfits in the choice of fixed or correlated parameters, qualitative methods using an alternative way of data handling may be useful, prior to the application of the fitting procedure. The phase derivative method, based on the analysis of the beat stemming from the combination of two close frequency sinusoids, has proved in several complex systems its usefulness as a diagnostic tool.<sup>23–25</sup> This method, by characterizing the occurrence of a distance splitting, should be especially useful to identify possible collapse of this splitting as the temperature is increased. With the support of this evidence, the EXAFS fitting analysis should then be specially focused on the behavior of the disorder-related Debye Waller-like term.

X-ray absorption near-edge spectroscopy (XANES) has been shown to be very sensitive to the various degrees of freedom governing the electronic properties of manganite compounds, such as local atomic distortion, charge transfer in the Mn–O bond, or local magnetic ordering.<sup>5–7,17–21</sup> The temperature dependence of XANES spectra in  $\text{LaMnO}_3$  has been the object of some reports in the literature,<sup>18–20</sup> but most of them are related to the thermal behavior of this compound around the magnetic ordering temperature ( $\sim 140$  K). It can be expected that the temperature dependence of XANES spectra across the orthorhombic to cubic transition may shed more light on the modification in the local atomic and electronic structure at the site of the  $\text{Mn}^{3+}$  ions.

We address here the issue of the temperature dependence of the local distortion around  $\text{Mn}^{3+}$  ions in  $\text{LaMnO}_3$  with a complete set of EXAFS and XANES data, collected below and above  $T^*$ . At this temperature some discontinuities are

observed in both the EXAFS and XANES range data. In the EXAFS range, the Jahn-Teller distance splitting still exists within the coordination shell even above the transition, but modification in the disorder can be identified. At low temperature the static disorder associated with the long bond  $(\text{Mn-O})_l$  is about 3 times larger than the disorder associated with the short bond  $(\text{Mn-O})_s$ . As the temperature increases the overall disorder associated with the short bond is rapidly dominated by the thermal contribution whereas the structural term is still dominant for the long bond. Around  $T^*$  these terms become of the same order and the thermal disorder is likely to be dominant for all apical and basal bonds. We conclude then that the tetragonal distortion is preserved across  $T^*$ , in agreement with an order-disorder character for the transition. We point out that this transition takes place when the relative displacement of the atoms along the long and short bonds becomes of the same order, turning the average radial disorder isotropic and allowing the bond length to vary independently. In the XANES range, the weak but significant discontinuities observed across  $T^*$  are associated with an increase of the covalent character of the Mn–O bonds.

## II. EXPERIMENT

The Mn–K edge EXAFS spectra were collected on a powder of  $\text{LaMnO}_3$  synthesized by the solid-state reaction method. The sample shows an orthorhombic to cubic transition at  $T^* \sim 710$  K. Details of the synthesis method, the structural characterization, and magnetic of the sample have been published elsewhere.<sup>11</sup> The temperature-dependent x-ray absorption measurements were performed at LNLS D04B-XAS1 beamline<sup>26</sup> in the transmission mode. A fine-grained powder sample of  $\text{LaMnO}_3$  was pressed between two thin beryllium windows and placed into an electrical furnace with low vacuum ( $<10^{-3}$  Torr). EXAFS and XANES data were collected at increasing temperature from 300 K to 870 K. Then the temperature has been decreased and the XAS spectra have been collected again at some temperature points and compared to those previously collected. Using this procedure we can certify that the sample had not been oxidized during the high-temperature measurements. In addition we verify with this procedure the perfect reproducibility of the subtle features in the XANES spectra. The EXAFS data were collected up to  $k_{max}=12.5 \text{ \AA}^{-1}$ . This data range limits the minimum difference between two close distances that can be resolved in the EXAFS analysis to the value  $(\delta R)_{min}=0.13 \text{ \AA}$ . The two distances at 1.91 Å and 1.97 Å are seen as one unique distance  $(\text{Mn-O})_s \approx 1.94 \text{ \AA}$ , easily resolved from the long distance  $(\text{Mn-O})_l \approx 2.15 \text{ \AA}$  ( $\delta R=0.21 \text{ \AA}$ ). The experimental resolution for the XANES experiments was about 1.5 eV. The simultaneous collection of XANES metal foil reference spectra enables the eventual correction of a small energy shift due to thermal effects in the optics of the beamline. After background subtraction the spectra were normalized in the range 150–250 eV above the edge. The features in the XANES spectra can then be compared in intensity and in position with a sensitivity as low as 0.1 eV.

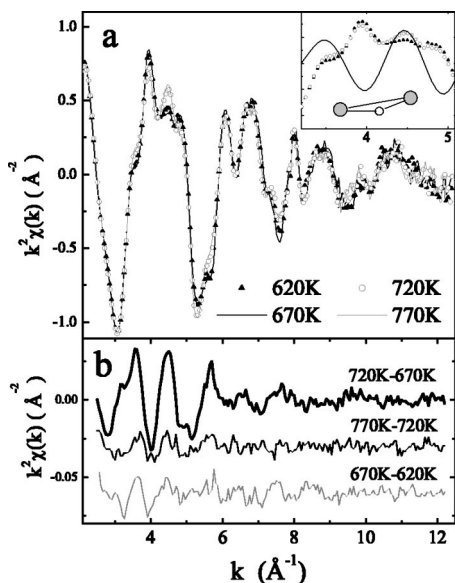


FIG. 1. EXAFS signal (a) and difference spectra (b) below, above, and across the transition temperature  $T^*$ . The inset is a close-up of the first EXAFS oscillation showing the simulation of the three-leg MS contribution, in phase with the main additional structure above the transition.

The EXAFS oscillations were extracted following standard procedure.<sup>27</sup> The signal corresponding to the oxygen coordination shell is selected by Fourier filtering. A first analysis has been made using the phase derivative (PD) method. This method is based on the exploration of the modulation in the EXAFS signal occurring when the contributions of two close shells separated by  $\delta R$  are combined. For close shells with the same backscattering atom, this modulation results in a minimum in the total amplitude and an inflection in the total phase of the EXAFS signal, at  $k = k_B$  given by  $k_B \sim \pi/2\delta R$  (Refs. 23–25). The presence of a beat is widely used to identify the occurrence of close shells. Due to the approximations involved,  $\delta R_B = \pi/2k_B$  does not give exactly the bond length separation; however, any relative modification in this separation will be detected by a shift in the beat position. The second analysis consisted in the application of the conventional fitting procedure constraining the parameters using the information obtained from the PD method. In the fitting procedure, the number of free parameters is limited to  $n \approx 7$  by the useful range and the interval corresponding to the selected signal in the real space.

### III. RESULTS AND DISCUSSION

The  $k^2$ -weighted  $\chi(k)$  spectra [ $\chi(k) * k^2$ ] for selected temperatures below and above the cell ordering temperature  $T^*$  ( $\sim 710$  K) are shown in Fig. 1(a). In Fig. 1(b), we report the difference EXAFS spectra for measurement at a temperature differing by 50 K, just below, just above, and across the transition. Subtle modifications are observed across  $T^*$ . The high frequency of these modifications indicates that they are associated with higher shells or multiple-scattering (MS) effects. We would like to call attention to the additional feature

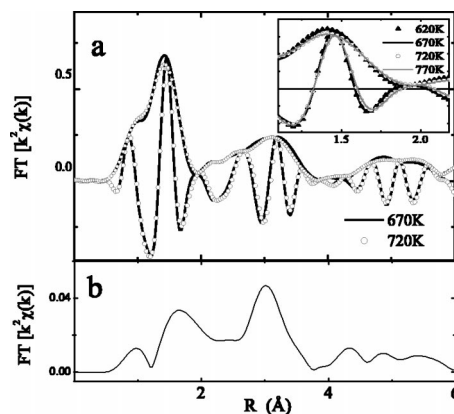


FIG. 2. (a) Fourier transform of the EXAFS signal across  $T^*$  (modulus and real part). Inset: detail of the first peak corresponding to the coordination shell. Subtle but reproducible changes are observed for temperatures below and above the transition temperature. (b) Modulus of the Fourier transform of the difference EXAFS signal across  $T^*$ , showing the two differential contributions around 3 and 1.8 Å.

appearing around  $k = 4.5 \text{ \AA}^{-1}$  in the EXAFS spectra [Fig. 1(a)]. This feature is common, with different scale of intensities, to all reported EXAFS spectra of manganite compounds, but is absent in  $\text{LaMnO}_3$  below  $T^*$  (Refs. 5–7, 14, and 15). Aiming to determine the exact origin of this contribution, we perform *ab initio* simulations in MS expansion, using the FEF7 code.<sup>28,29</sup> Different clusters were built using the crystallographic structure of  $Pbnm$  and  $R\bar{3}C$  doped compounds. A path-by-path study allowed the identification of the additional contribution above  $T^*$  as being mainly due to three-leg MS paths involving two neighboring Mn atoms and their common oxygen [Fig. 1(a), inset]. The contribution of this path increases with increasing the superexchange angle (tilt angle) Mn–O–Mn, as well as with the reduction of angular disorder. This contribution is clearly revealed in the Fourier transform (FT) of the EXAFS signal across  $T^*$  (Fig. 2). Apart from other modifications, discussed below, a large peak around 3 Å corresponding to that MS contribution, shows up in the difference signal [Fig. 2(b)]. As neutron diffraction studies<sup>8</sup> do contain any report of an anomalous behavior in the average tilt angle, we may conclude that the enhancement of the MS contribution at  $T^*$  is more likely related to a reduction of the average angular disorder.

A closer view of the first peak in FT corresponding to the contribution of the coordination shell [Fig. 2(a), inset] reveals small but significant modifications occurring within the  $\text{MnO}_6$  octahedra, across the transition. The shape of the signal is not notably affected, but we observe a small drop in the height of the peak (at  $\sim 1.3$  Å) and a discontinuity in the real FT component, in the high- $R$  side of the peak (at  $\sim 1.8$  Å), associated with the long-bond contribution.<sup>7</sup> The Fourier transform of the difference spectra across  $T^*$  [Fig. 2(b)] shows a peak around 1.8 Å, confirming the occurrence of a structural modification within the coordination shell. As already pointed out, the thermal damping may smooth and screen part of the real effects, so that a thorough analysis is necessary to determine

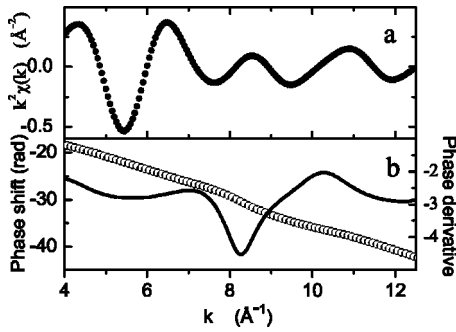


FIG. 3. (a) Back-Fourier-transformed signal of the coordination shell at room temperature. (b) Total phase shift and derivative: the minimum of the curve defines the beat position  $k_B$ .

the extent of modification of the local atomic organization.

The PD method was applied in the analysis of this coordination shell contribution, first for the room-temperature (RT) spectrum, where the local structure is already well established. The EXAFS signal was back Fourier transformed in the  $R$  range 0.7–2.1 Å [Fig. 3(a)]. A minimum in the total amplitude [Fig. 3(a)] and an inflection point in the total phase [Fig. 3(b)] are observed at  $k_B=8.3$  Å<sup>-1</sup>. This beat position corresponds to a value  $\delta R_B=\pi/2k_B=0.19$  Å, in good agreement with bond length separation obtained from crystallographic data ( $\delta R=0.21$  Å). The small difference, most likely due to the approximations involved in the PD method,<sup>23</sup> is commonly reported<sup>24,25</sup> and does not affect the precision in the relative modification of this separation, which should be revealed by a shift in the beat position. Identical procedures of the phase extraction have been applied to the EXAFS spectra in the whole temperature range, leading to a beat position value comprised between 8.1 and 8.5 Å<sup>-1</sup> [Fig. 4(a)]. A relative error of 5% has been estimated from the mean-square deviation for spectra collected at the same temperature. Within this error bar the same value of  $k_B$  is obtained over the whole temperature range, showing that the bond length splitting is kept constant across  $T^*$  [Fig. 4(b)].

A two-shell fit in  $k$  space is then performed using theoretical amplitude and phase functions generated using the FEFF7 code<sup>28,29</sup> from the crystallographic  $Pbnm$  structure of LaMnO<sub>3</sub>. The number of first neighbors were fixed [ $N_1=4$  for the short (Mn–O)<sub>s</sub> bonds and  $N_2=2$  for the (Mn–O)<sub>l</sub> long bonds] and the value of the amplitude reduction factor  $S_0^2$  was determined from RT spectra and then fixed for the analysis of the spectra at other temperatures. Figure 5 shows the results of the fit. We note that the Mn–O distances remain almost constant through  $T^*$  at values close to those known for LaMnO<sub>3</sub> at RT: (Mn–O)<sub>s</sub>=1.93 Å and (Mn–O)<sub>l</sub>=2.15 Å, confirming that there is no collapse of these distances across the transition.

As concerns the disorder, the study of the Debye-Waller term brings about some interesting observations. As already been pointed out in previous XAS studies,<sup>6,7</sup> the disorder associated with the long and short bonds at room temperature are quite different. According to the prediction of Goodenough<sup>30</sup> about the character of the Mn–O bonding, the short (Mn–O)<sub>s</sub> bonds are stable bonds with semicovalent

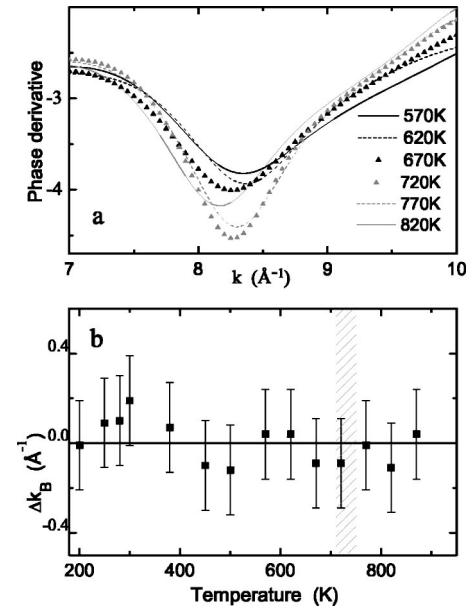


FIG. 4. (a) Total phase shift derivative: the minimum of the curve defines the beat position  $k_B$ . (b) Variation of the  $k_B$  value with the temperature. The domain where the orthorhombic to cubic transition takes place is marked by the hatched area.

character, while the long (Mn–O)<sub>l</sub> distance corresponds to a weaker ionic bonding. The static radial disorder associated with the ionic long bonds is large ( $\sigma=0.07$  Å) and keeps almost the same value over the whole temperature range below  $T^*$ . The radial disorder associated with the short bonds is about 3 times smaller at room temperature, in agreement with the results reported in the literature. The evolution of this factor is thermally driven, well accounted for by a simple correlated model for the thermal vibrations.<sup>22</sup> The temperature found for the Einstein model is  $\Theta_E\sim 680$  K (Fig. 5), in agreement with the high Debye temperatures ( $\Theta_D\sim 3/2\Theta_E\sim 1000$  K) already reported in perovskites

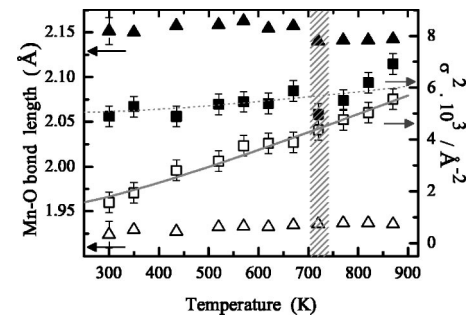


FIG. 5. Mn–O bond lengths (triangles, left scale) and associated DWF's (square, right scale). The open symbols and solid symbols correspond to short and long lengths, respectively. For the sake of clarity the error bars in the bond lengths, almost constant over the temperature range, have been shown only for room temperature. The solid line is the fit of the thermal disorder using the correlated Einstein model. The dotted line is only a guide for the eyes. A small drop of the long-bond DWF is observed at  $T^*$  (hatched area). At this temperature the DWF's of the short and long bonds are equalized.

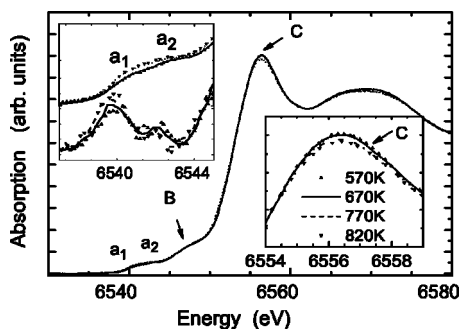


FIG. 6. XANES spectra across the orbital ordering temperature ( $\sim 710$  K). The insets are close views showing the subtle discontinuities in amplitude. Left inset: pre-edge region and corresponding absorption derivative. Right inset: main feature C.

compounds.<sup>2,18</sup> The DWF associated with long bonds is almost temperature independent up to values close to  $T^*$ . At this temperature we observe a small drop in this factor, partially screened by the error on the determination of  $\sigma^2$ . We should point out that at this temperature the DWF's associated with short and long bonds assume essentially the same values. Above  $T^*$  both factors seem to follow a simple thermal behavior, in the continuity of the low-temperature behavior of the short-bond DWF.

The small drop in the long-bond DWF is consistent with the small discontinuity in the long-bond-related side in the FT (Fig. 2). As the distances are kept constant and the DWF associated with the short bond increases continuously, it should be related to the drop in the height of the peak in the FT across the transition. We should emphasize that the DWF in EXAFS only accounts for radial disorder—i.e., the relative variation in the Mn and O positions—projected along the bond axis. In the basal plane, all the Mn–O–Mn linkages are composed of a long and a short bond. The longitudinal variation of the  $(\text{Mn–O})_l$  length should then be accommodated by flattening and unbending the Mn–O–Mn angle. The resulting transverse accommodation has a limited projection on the  $(\text{Mn–O})_s$  bond and is not “seen” in the radial disorder term. Additionally, the accommodation through the Mn–O–Mn angle yields to destructive interferences in the different multiple-scattering contributions of the almost linear three-leg MS paths [Fig. 1(a), inset] and limits the total contribution to the EXAFS signal. Around  $T^*$  the radial DWF of  $(\text{Mn–O})_s$  bonds becomes of the same order as that of  $(\text{Mn–O})_l$  bonds and the variations of the short and long bonds are almost decorrelated. The two terms follow then similar thermal behaviors. The Mn–O–Mn angle is no longer so strongly involved in the accommodation of the bond vibrations and the contribution of the multiple-scattering path involving the two adjacent Mn and their common O increases. The reduction of the angular distortion favors an increase of the hybridization between the Mn  $3d$  and O  $2p$  orbitals.

The XANES spectra across the transition (570–820 K) are shown in Fig. 6. The spectra exhibit the features already reported in  $\text{LaMnO}_3$  (Refs. 17–21). The two pre-edge peaks  $a_1$  and  $a_2$  (6540.0 and 6542.4 eV) arise essentially from  $1s$ - $4p$  dipole-allowed transitions of Mn  $3d$  character. They

account for the hybridization of the Mn  $4p$  orbitals with the Mn  $3d$  orbitals on neighboring Mn ions, either directly or via O atoms.<sup>31,32</sup> In reduced symmetry due to the local Jahn-Teller distortion of the  $\text{MnO}_6$  octahedra, the  $1s \rightarrow 4p$  transition on Mn site is split into separable components close to the onset (shoulder B) around 6546 eV and at the top of the rising edge (C main peak) in the region 6550–6560 eV where lies most of the spectral strength.<sup>18</sup> There is no energy shift in the XANES over the whole temperature range, in agreement with the absence of significant modification in the average coordination distance. It has been recently invoked<sup>33</sup> that a charge disproportionation for the Mn ions could happen at the transition temperature. However, this would result in a splitting in the rising edge that has not been observed. Drastic changes in the charge disproportionation should then be excluded. The top of the main feature C measures the net  $4p$  hole count. Up to the transition temperature the intensity of this C peak decreases very slowly and continuously when the temperature increases as a consequence of the increase of the thermal disorder. At the transition a small additional drop in the maximum peak height takes place (Fig. 6, inset). We should remind the reader that the experimental procedure based on the collection of the XAS data twice, both at increasing and decreasing temperatures, assures us the perfect reproducibility of the XANES features. Small changes in the intensity of the features, especially in the maximum peak height, are not experimental artifacts. An additional drop in the hole count is then observed across the transition. It accounts for an additional nonthermal increase of the delocalization of the  $e_g$  electrons through a band effect associated to the increase of the average Mn–O bond covalence.<sup>31</sup> Correlatively, subtle but reproducible modifications are observed in the pre-edge domain (Fig. 6, inset). Alterations in the spectral weight of these features are currently associated with modification in the distribution of  $e_g$  majority and ( $e_g t_{2g}$ ) minority states.<sup>18</sup> In the present case we do not observe spectral transfer from one to the other features, but the simultaneous enhancement of the two features. We associate this enhancement with an increase of the hybridization between the Mn  $4p$  orbitals and the Mn  $3d$  orbitals on neighboring atoms. This is consistent with a reduction of the disorder in the superexchange angle deduced from EXAFS analysis. The delocalization of the  $e_g$  electrons due to the thermal disorder partly overcomes the localization associated with the ionic bonds and should be related to the reported drop in the resistivity at the orbital ordering temperature.<sup>9,21</sup>

#### IV. CONCLUSIONS

We reported an XAS study of the local atomic and structural modifications around the manganese atoms in  $\text{LaMnO}_3$  across the orbital ordering transition  $T^*$ . The Jahn-Teller splitting into long  $(\text{Mn–O})_l$  and short  $(\text{Mn–O})_s$  bonds within the  $\text{MnO}_6$  octahedra is kept in the high-temperature phase. We observe that significant electronic and structural changes are taking place across this transition at the Mn site. We show that the structural modifications correspond to a change in the accommodation of the local thermal disorder related to vibrations of the Mn–O bonds. We point out that the orbital

ordering transition takes place when the relative displacement of the atoms along the long and short bonds becomes of the same order. Below  $T^*$ , the radial thermal disorder appears to be mostly accommodated by a bending of the tilt angle Mn–O–Mn among adjacent octahedra. Above  $T^*$ , the Mn–O–Mn angles are flattened and strengthened and the average radial disorder becomes isotropic, allowing a complete decorrelation of the bond length variations. Subtle electronic modifications at the Mn sites also take place: a small drop in the  $4p$  counts and a small enhancement of the hy-

bridization between  $4p$  and  $3p$  orbitals are observed across the transition. These modifications are associated with an increase of the average covalent character of the Mn–O bonds.

#### ACKNOWLEDGMENTS

This work is partially supported by LNLS/ABTLuS/MCT. R.A.S. acknowledges the PIBIC/CNPq. A.Y.R. acknowledges a grant from CNPq/PCI.

\*Electronic address: aramos@lnls.br

- <sup>1</sup>A. J. Millis, *Nature (London)* **392**, 147 (1998).
- <sup>2</sup>T. Proffen, R. Francesco, S. Billinge, E. Brosha, and G. Kwei, *Phys. Rev. B* **60**, 9973 (1999).
- <sup>3</sup>S. Billinge, T. Proffen, V. Petkov, J. L. Sarrao, and S. Kycia, *Phys. Rev. B* **62**, 1203 (2000).
- <sup>4</sup>D. Louca, E. Brosha, and T. Egami, *Phys. Rev. B* **61**, 1351 (2000).
- <sup>5</sup>C. H. Booth, F. Bridges, G. Kwei, J. M. Lawrence, A. L. Cornelius, and J. Neumeier, *Phys. Rev. B* **57**, 10 440 (1998).
- <sup>6</sup>G. Subías, J. García, J. Blasco, and M. Proietti, *Phys. Rev. B* **58**, 9287 (1998).
- <sup>7</sup>T. Shibata, B. Bunker, and J. F. Mitchell, *Phys. Rev. B* **68**, 024103 (2003).
- <sup>8</sup>J. Rodriguez-Carvajal, M. Hennion, F. Moussa, A. Moudén, L. Pinsart, and A. Revcolevschi, *Phys. Rev. B* **57**, R3189 (1998).
- <sup>9</sup>J.-S. Zhou and J. Goodenough, *Phys. Rev. B* **60**, R15 002 (1999).
- <sup>10</sup>A. Millis, *Phys. Rev. B* **53**, 8434 (1996).
- <sup>11</sup>E. Granado, J. A. Sanjurjo, C. Rettori, J. Neumeier, and S. Oseroff, *Phys. Rev. B* **62**, 11 304 (2000).
- <sup>12</sup>E. Araya-Rodriguez, A. Y. Ramos, H. C. N. Tolentino, E. Granado, and S. Oseroff, *J. Magn. Magn. Mater.* **233**, 88 (2001).
- <sup>13</sup>J. Song, J. Park, K. Lee, J. Lee, and Y. Jeong, *Phys. Rev. B* **66**, 020407(R) (2002).
- <sup>14</sup>M. Sánchez, G. Subías, J. García, and J. Blasco, *Phys. Rev. Lett.* **90**, 045503 (2003).
- <sup>15</sup>T. A. Tyson, J. M. de Leon, S. D. Conradson, A. R. Bishop, J. J. Neumeier, H. Röder, and J. Zang, *Phys. Rev. B* **53**, 13 985 (1996).
- <sup>16</sup>A. Lanzara, N. Saini, M. Brunelli, F. Natali, A. Bianconi, P. Radaelli, and S. Cheong, *Phys. Rev. Lett.* **81**, 878 (1998).
- <sup>17</sup>M. Croft, D. Sills, M. Greenblatt, C. Lee, S.-W. Cheong, K. Ramanujachary, and D. Tran, *Phys. Rev. B* **55**, 8726 (1997).
- <sup>18</sup>F. Bridges, C. H. Booth, G. Kwei, J. Neumeier, and G. Sawatzky, *Phys. Rev. B* **61**, R9237 (2000).
- <sup>19</sup>F. Bridges, C. H. Booth, M. Anderson, G. Kwei, J. Neumeier, J. Snyder, J. Mitchell, J. Gardner, and E. Brosha, *Phys. Rev. B* **63**, 214405 (2001).
- <sup>20</sup>Q. Qian, T. A. Tyson, C.-C. Kao, M. Croft, S.-W. Cheong, and M. Greenblatt, *Phys. Rev. B* **62**, 13 472 (2000).
- <sup>21</sup>Q. Qian, T. A. Tyson, S. Savrassov, C.-C. Kao, and M. Croft, *Phys. Rev. B* **68**, 014429 (2003).
- <sup>22</sup>E. Sevillano, H. Meuth, and J. J. Rehr, *Phys. Rev. B* **20**, 4908 (1979).
- <sup>23</sup>G. Martens, P. Rabe, N. Schwentner, and A. Werner, *Phys. Rev. Lett.* **39**, 1411 (1977).
- <sup>24</sup>H. Jaffres *et al.*, *Phys. Rev. B* **61**, 14 628 (2000).
- <sup>25</sup>D. Jiang, E. Crozier, and B. Heinrich, *Phys. Rev. B* **44**, 6401 (1991).
- <sup>26</sup>H. C. N. Tolentino, A. Y. Ramos, M. C. M. Alves, R. A. Barrea, E. Tamura, J. C. Cezar, and N. Watanabe, *J. Synchrotron Radiat.* **8**, 1040 (2001).
- <sup>27</sup>*X-Ray Absorption: Principles, Applications, Techniques of EXAFS, SEXAFS and XANES*, edited by D. C. Koningsberger and R. Prins, Vol. 92 of Chemical Analysis (Wiley, New York, 1988).
- <sup>28</sup>J. J. Rehr, J. M. de Leon, S. Zabinsky, and R. C. Albers, *J. Am. Chem. Soc.* **113**, 5135 (1991).
- <sup>29</sup>J. J. Rehr, R. C. Albers, and S. Zabinsky, *Phys. Rev. Lett.* **69**, 3397 (1992).
- <sup>30</sup>J. Goodenough, *Phys. Rev.* **100**, 564 (1955).
- <sup>31</sup>I. S. Elfimov, V. I. Anisimov, and G. A. Sawatzky, *Phys. Rev. Lett.* **82**, 4264 (1999).
- <sup>32</sup>L. Hozoi, A. de Vries, and R. Broer, *Phys. Rev. B* **64**, 165104 (2001).
- <sup>33</sup>J.-S. Zhou and J. Goodenough, *Phys. Rev. B* **68**, 144406 (2003).